Soft Matter

PAPER

View Article Online
View Journal | View Issue

Cite this: *Soft Matter*, 2014, **10**, 5797

Stabilisation of 2D colloidal assemblies by polymerisation of liquid crystalline matrices for photonic applications

Giorgio Mirri,*[ab] V. S. R. Jampani,[a] George Cordoyiannis,[a] Polona Umek,[a] Paul H. J. Kouwer*[b] and Igor Muševič*[ac]

Received 14th February 2014
Accepted 27th May 2014

DOI: 10.1039/c4sm00358f

www.rsc.org/softmatter

Colloidal crystals in anisotropic matrices are extremely stable and versatile, but disassemble as soon as the anisotropy of the matrix disappears. We present an approach to first custom-assemble colloidal structures and subsequently stabilize them through photo-polymerisation of the liquid crystalline matrix. The resulting 2D colloidal assemblies are stable at high temperatures and can even be obtained as free-standing films without a decrease in the degree of organization. This approach could be used to stabilize and extract recently proposed soft-matter photonic microcircuits based on liquid crystal optical microresonators, microlasers and microfibers, and opens up routes towards real soft matter photonic devices that are stable over extended time and temperatures.

Introduction

Water based colloidal crystals have been of great interest for their possible application as photonic materials. Bottom-up assembly of colloids in isotropic media like water is governed by a balance between the electrostatic repulsive forces and van der Waals attractive interaction.[1–4] In addition to this classical mechanism of interaction, colloidal interaction driven by osmotic pressure generated by depletion of non-interacting nano-particles or molecules has also been observed and reported.[5,6] Control of the structures formed in isotropic media is achievable by using sophisticated techniques, such as photolithography, photo-etching and focused ion beam etching.[7–9] Anisotropic interaction in isotropic media has been achieved with non-spherical particles using polymer depletion aggregation[10,11] or anisotropic selective interactions.[12]

Assembling solid colloids, liquid or gas emulsions in liquid crystals (LCs) was explored in the past decade.[13] While colloidal interactions are spatially isotropic in water-based dispersions, colloidal interactions are strongly anisotropic in orientationally ordered anisotropic media, such as liquid crystals.[14] The boundary conditions for the orientation of LC molecules at the surface of the cell (*i.e.* the device constituted by two glasses treated with an aligning agent to govern the general alignment of the LC) and at the particles generate defects in the LC host/solvent, *i.e.* areas characterized by a lower orientational order. The formation of defects on nematic droplets of a calamitic liquid crystal in a discotic one was reported by Pratibha *et al.*,[15] Poulin *et al.*[16] reported the self-assembly of water droplets in nematic LCs by sharing the defect areas in order to minimize the elastic distortion of the whole system. Recently, Muševič *et al.*[17,18] reported a method to guide the self-assembly process to obtain 2D and 3D ordered structures of silica colloids in the nematic liquid crystals by means of laser tweezers. This method allows a one-by-one assembly of a colloidal crystal. Optical trapping of micrometer-sized objects by a laser beam was first demonstrated by Ashkin in 1970[19] showing that transparent objects with a higher refractive index than the surrounding media are attracted into the focus of a laser beam. This method is nowadays widely used in colloidal science and technology.[20]

A similar effect was observed when trapping high refractive index colloids in low refractive index liquid crystals.[21,22] Later, it was reported that in anisotropic and ordered media, such as liquid crystals, even objects with a lower refractive index than the surrounding liquid could be trapped by laser beams.[23,24] This "forbidden" trapping is inherently related to the optical anisotropy of liquid crystals and relies on two different mechanisms; (a) the refractive index around the colloid is increased by the distortion of the medium around the low-refractive index particles; and (b) the distortion of the liquid crystal medium caused by the electric field of focused laser which behaves like a ghost colloid.

These effects disappear when the nematic media are heated to the isotropic phase and the ordinary trapping mechanism is observed. Recently, Škarabot *et al.* reported another mechanism for trapping nematic colloids by means of laser tweezers. In this

[a]*Soft Matter Materials Lab, Solid State Physics Department, Jožef Stefan Institute, Jamova cesta 39, 1000, Ljubljana, Slovenia. E-mail: igor.musevic@ijs.si; giorgio.mirri@ijs.si*

[b]*Institute for Molecules and Materials, Radboud University Nijmegen, Heyendaalseweg 135, 6525 AJ, Nijmegen, The Netherlands*

[c]*Faculty of Mathematics and Physics, University of Ljubljana, Jadranska 19, 1000, Ljubljana, Slovenia*

case the liquid crystal is locally heated, so that the degree of orientational order is locally reduced. The resulting gradient of the order parameter generates a force on a colloidal particle, trapping the particles in the region of reduced order. Interestingly, this gradient force is effective down to a molecular scale, so that even larger molecules could be trapped.[25] In our experiments, we are using local heating and melting of a liquid crystal by the intense light of the laser tweezers to create a small "island" of the isotropic phase, which is surrounded by the nematic phase. Because the isotropic–nematic phase transition is of first order, there is a sharp interface, dividing both phases. This interface strongly attracts particles in liquid crystals, regardless of their refractive index, surface properties, size or shape.

Furthermore, optical tweezers were used to knit the chiral topologically interlocked structures of defects arising in 2D colloidal crystals assembled in chiral nematic LCs opening new features in the topology of soft matter.[26,27] The assemblies generated in aligned LCs are highly stable; the interparticle interactions are in fact of the order of 1000 k_BT. However, in all the cases described the forces responsible of keeping the assembly bound are intrinsically related to the anisotropy and alignment of the LC media, therefore, these assemblies are stable only in the liquid crystalline matrix where they are generated. In other words, disappearance of the liquid crystalline order caused by heat (*i.e.* melting of the LC phase) or by removal of the boundary conditions (*i.e.* opening the cell) would result in disassembly of the colloidal crystal.

Here we present a method to stabilize 2D colloidal assemblies up to ≥150 °C, *i.e.* much higher temperatures than the clearing temperature of many commercial liquid crystals, using a polymerisable LC medium, composed of LC acrylate monomers and a photo-initiator dissolved in 4-cyano-4′-pentylbiphenyl (5CB). Polymerisation of a mixture of mono and bifunctional acrylate monomers results in the formation of a polymer network, which retains the original alignment of the unpolymerised matrix.[28] A schematic representation of the network formation process is shown in Fig. 1. LC polymer networks unify the optical anisotropy of liquid crystals with the dimensional stability and flexibility of polymers/elastomers. For this reason they have been used for a wide range of applications from LCDs to sensors and actuators,[28,29] and to confer chirality to achiral nematic in order to obtain photonic band gaps.[30] In addition, polymer networks have been applied to stabilize blue phases[31] and to generate patterns of silver nanoparticles.[32] Using a photo-polymerisation approach, we present a straightforward method to first employ the low viscosity of the LC monomer solution to build well-defined colloidal crystals, and second, to capture them in a polymer network. We demonstrate that the colloidal assemblies retain their structure at elevated temperatures where conventional LC colloidal dispersion would disassemble. In addition, we show that we are able to open the preparation cell and obtain free standing colloidal structures, which commonly are only available by photolithographic techniques.

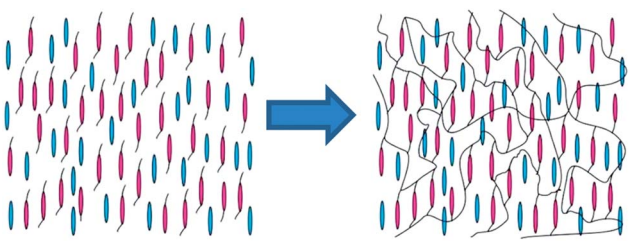

Fig. 1 Pictorial representation of the polymerisation of reactive mesogens. Reactive mesogen molecules are represented in pink; non-reactive mesogen molecules are represented in blue.

Experiments and discussion

Materials and assembling methods

As the LC host medium, we used RM305 (12.5 wt%), RM257 (12.5 wt%, both obtained from Merck Ltd., Southampton, UK) and a photo-initiator (IRGACURE 907, 0.1 wt%, BASF, Germany) in the nematic LC 4-pentyl-4′-cyanobiphenyl (5CB). Silica microspheres with a diameter of 3.1, 5.01 or 7.3 μm (Bangs Labs, USA) were chemically treated with dimethyloctadecyl[3-(trimethoxysilyl)propyl]ammonium chloride (DMOAP, ABCR Germany). After silanisation, a monolayer of DMOAP is formed on the surface, which induces a homeotropic (perpendicular) alignment of the LC molecules on the colloid surface. The silanised silica microspheres were mixed with the reactive LC medium and colloidal dispersion was introduced by capillary force into a cell, constituted of two glass slides, each of them having a thin layer of indium-tin-oxide (ITO), covered by a thin layer of spin-coated polyimide (PI-2555, NISSAN Chemicals). Before the cell was assembled, the PI layer was rubbed onto a soft velvet cloth according to the lab procedure to confer good macroscopic planar alignment, with the liquid crystal molecules oriented parallel to the PI surface and along the rubbing direction. In line with previous observations, we found that homeotropic colloids in the planar nematic cell give rise to two different kinds of topological defects. In thicker parts of the cell, dipolar colloids were observed, where each colloidal particle is accompanied by a hedgehog (point) defect. This configuration is also called an elastic dipole and resembles an electric dipole. In thinner parts of the cell, quadrupolar colloids are observed, where each colloidal particle is encircled by a Saturn ring, resembling an electric quadrupole.[14]

Elastic dipoles and quadrupoles in the nematic liquid crystal attract each other, forming linear or kinked chains, which can be assembled into 2D dipolar or quadrupolar nematic colloidal crystals[17] and 3D dipolar colloidal crystals.[18] The reason for this colloidal interaction in the nematic liquid crystals is quite different from colloidal interactions in water-based colloids; the electrostatic and van der Waals forces can safely be neglected. Colloidal pair interaction is in this case due to elastically distorted liquid crystals around each colloidal particle. This deformed region can extend up to ten micrometers from a micrometer-sized particle and can easily be observed under a polarizing optical microscope. When two particles are close enough, their elastically deformed regions start to overlap and this creates very strong and long range colloidal interaction. The

particles are attracted to minimize the deformation energy and they form chains, such as those in Fig. 2. The binding energies are of the order of several 1000 k_BT per micrometer diameter colloid.

For this study we focused on the assembly generated by the topological dipoles, which self-assemble into colloidal chains, oriented parallel to the rubbing direction (Fig. 2).[17] For the assembly process we used optical tweezers based on an Nd-YAG laser (1064 nm), which does not initiate polymerisation. Colloidal manipulation was facilitated by local heating caused by absorption of the ITO layer. The nematic LC is locally molten at high-enough laser power, which generates a tens-of-micrometer diameter isotropic island. As shown in Fig. 2, the isotropic island generated by the laser attracts the colloidal chains, which were previously assembled in the same cell. The laser power was adjusted during the experiment in order to control the assembly process and not to disrupt the order of the colloidal crystal already assembled. In fact, when the laser is directed on the assembly before polymerisation, colloidal particles may detach from it, and the colloidal assembly can be disrupted (Fig. 3). This happens because the isotropic island eliminates the elastic forces that keep the colloidal crystal together and because the isotropic–nematic interface strongly captures the particles. The right panel in Fig. 3 shows the effect of the isotropic island on the colloidal assembly. In this case the attracted particles outside the isotropic area are blocked by the interphase barrier at the borders of the isotropic droplet. This barrier also prevents particles inside the isotropic area, to escape from the island (these colloids are not in an anisotropic medium and, given their refractive index, are repelled by the laser).

After assembly of the colloidal crystals, the cell was irradiated with UV light (366 nm, 6 W, Köhler, Germany), which initiated the photo-polymerisation reaction. Irradiation was continued for 1 minute at a 2 cm distance from the cell. Fig. 4 shows a colloidal assembly after photo-polymerisation of the reactive LC host. Although the IR laser was passed directly onto it, the colloidal crystal remains completely unaltered. Between crossed polarizers, the isotropic island generated in a normal nematic LC by the IR laser should appear black, and the defects should not be recognizable. However, after polymerisation of the matrix the laser does not alter the alignment of the liquid crystalline network any longer. The isotropic island was not observable and even the defect structure of the colloidal assembly (Fig. 4a and b) was unaltered in the presence of the laser tweezers.

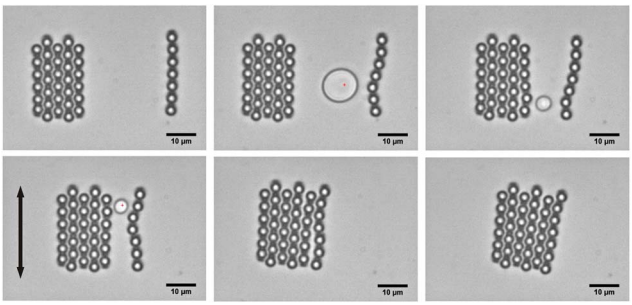

Fig. 2 Sequence of optical microscopy images, showing the optical tweezers assisted assembly of chains of 3.1 μm DMOAP-functionalized silica microspheres in the reactive LC medium. The circular object on the images is the isotropic island produced by the laser tweezers. The maximum laser power is approximately 385 mW. The red cross indicates the position of the laser tweezers focus. The scale bar is 10 μm. The black double headed arrow indicates the rubbing direction, *i.e.* the nematic director far away from the colloidal particles.

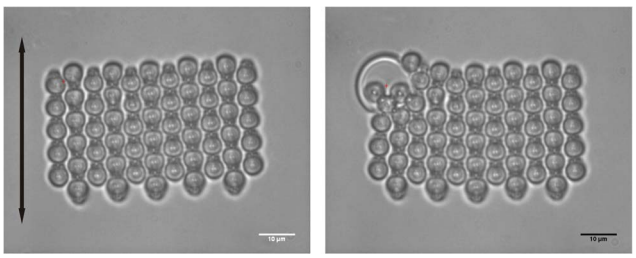

Fig. 3 Optical microscopy images of a colloidal crystal of 5.01 μm DMOAP-silica colloids in the reactive LC medium. The right image shows the disruptive effect of laser tweezers on the assembly. The laser power is approximately 385 mW. The molten island in the left upper corner of the colloidal assembly is the isotropic phase of the LC host. The black arrow indicates the rubbing direction.

Stability of the assemblies

The thermal stability of the liquid crystalline polymer network was also assessed by variable temperature optical polarization microscopy (OPM) and AC calorimetry. Fig. 5 shows the OPM images of the colloidal crystals embedded in a polymerised LC matrix as a function of temperature, through a retardation plate.[33] At 150 °C, the highest temperature accessible by our setup, the colloidal crystal has not changed. The only notable difference is the change in the colour of the thin rim around the colloidal crystal with increasing temperature. Fig. 6 shows the dimensions of the assembly in Fig. 5 before the polymer network is generated, after the polymerisation and of the polymerised sample at 150 °C.

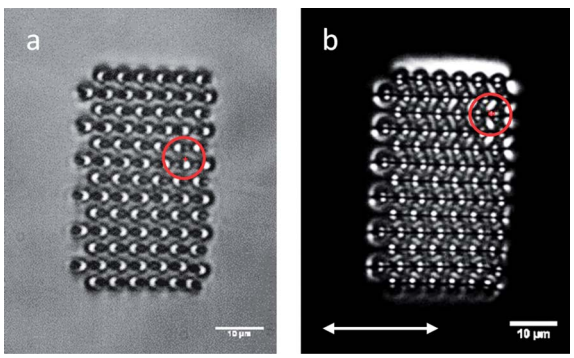

Fig. 4 Optical microscopy images of a single colloidal assembly of 3.13 μm silica beads in a photo-polymerised nematic matrix. The image of the sample between open parallel polarisers (a) and cross polarizers (b) shows that neither the assembly, nor the defect lines are impacted by the laser tweezers. The center of the laser beam is at the center of the red circle.

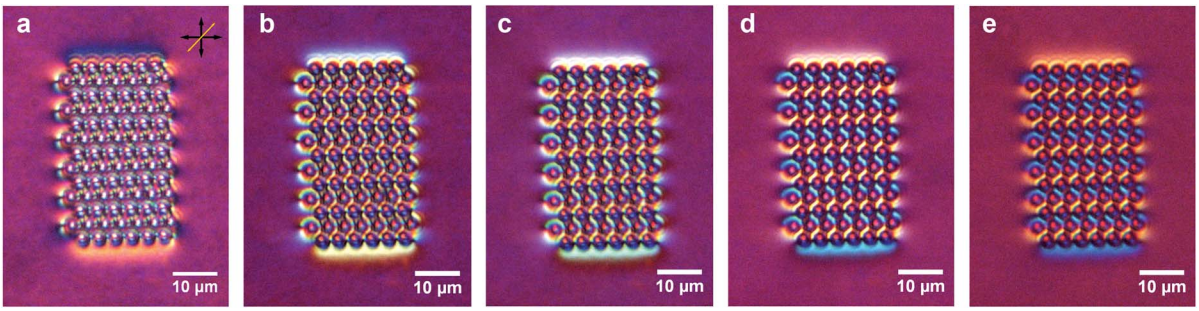

Fig. 5 Optical microscopy images of a colloidal crystal of 3.1 μm silica particles embedded in a polymerised nematic matrix, imaged between crossed polarizers with a retardation plate added at different temperatures. The colors indicate the orientation of the optical axis of the material and therefore also the orientation of molecules around the colloidal assembly. (a) 47 °C; (b) 71 °C; (c) 92 °C; (d) 133 °C and (e) >150 °C, which is the maximum allowed temperature of the thermistor used to measure the temperature. The black arrows indicate the direction of the polarizer and analyzer, the yellow arrow indicates the direction of the slow axis of the red retardation plate.

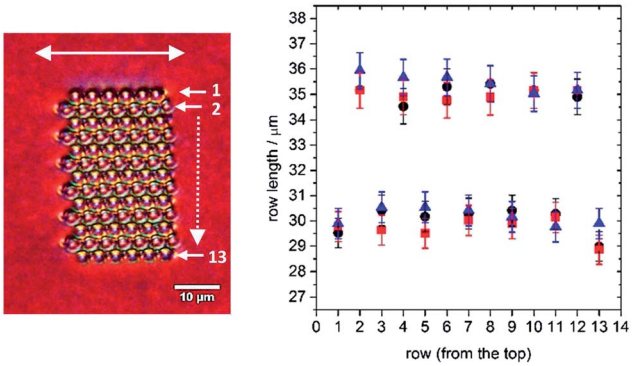

Fig. 6 (left) OPM image of a colloidal crystal of 3.1 μm DMOAP-microspheres (left panel) in polymerised LC matrix at room temperature, in the presence of a retardation plate. (right) Row lengths of the colloidal crystal before (black circles) and after (red squares) polymerisation at room temperature and after polymerisation at 150 °C (blue triangles). The rows are indicated in (a).

AC calorimetry studies and birefringence of the polymer network

The insertion of a retardation plate in the optical path with the slow axis at 45° gives the information about the local orientation of the liquid crystal molecules. In a 5CB cell, with a thickness comparable to the one used for our experiments (between 5 and 20 μm), a yellow colour is due to the orientation of the nematic director parallel to the slow axis of the retardation plate. The areas, where the director is oriented perpendicular to the slow axis of the retardation plate will appear blue. For a better comprehension of the discussion, it is worth underlining that this colour indication directly depends on the birefringence value and on the thickness of the sample, *i.e.* total retardation of the sample. Therefore, the change in the colour can be due to a mere change of the birefringence with the increasing temperature or, in the case the birefringence of the sample remains constant, to a change of the boundary conditions at the particles' surface due to surface melting of the alkyl chains. In the latter case the orientation at the colloid surface would change from homeotropic to planar which induces a change of the orientation of the nematic director around the assembly. To investigate this behaviour both a calorimetric study and a measurement of the birefringence at different temperatures was carried out. High-resolution AC calorimetry was used in order to reveal the thermal behaviour of samples. We used an in-house-developed and built computer-controlled setup, which is able to accurately probe the temperature dependence of the heat capacity. In this method an ac oscillating power of frequency ω is applied on the sample, which is thermally linked to the surrounding bath. A proper frequency is chosen to eliminate any temperature gradients in the sample. The heat capacity is calculated as a function of the input power, the frequency ω and the amplitude of sample's temperature oscillations.[34] This method has been extensively used for studies of phase transitions and critical phenomena in soft and solid materials.[35,36] Among the advantages of AC calorimetry one could mention its high sensitivity to even small changes of heat capacity. This method typically operates with slow scanning rates (down to few mK h^{-1}), thus reducing the rounding effects and yielding the precise temperature profiles of heat capacity. It can also distinguish between the first and second order phase transitions. For the calorimetric measurements, a 50 mg sample was placed in high-purity silver cells. Prior to the experiment all the cell components (silver cup and lid, indium paste, heater and thermistor) were weighed and their contribution to the total measured heat capacity was calculated and subtracted. The result was then divided by the mass of the sample, yielding its net specific heat capacity. Scanning rates of 1 K h^{-1} were used for our samples.

Thermal analysis of the polymerized sample (with increased content of reactive groups) in the absence of microparticles shows an increase of 5CB clearing temperature. In pure 5CB, the temperature of the nematic–isotropic phase transition is at $T_{NI,5CB} = 35$ °C, whereas in a polymerized matrix, the phase transition temperature of 5CB is increased to 50 °C, as shown in Fig. 6a. The increase is due to the presence of the liquid crystalline network which confines the nematic phase of 5CB and therefore increases its stability. One can clearly see another peak at 172 °C, which is attributed to the nematic–isotropic phase transition of the polymer network itself. When the particles are added and the sample is polymerized, the 5CB

clearing temperature shifts to even higher temperature (~65 °C), indicating the increase of confinement. However, the nematic–isotropic transition temperature of the polymer network is not affected by the presence of the particles. New transition peaks are observed in the presence of silica colloids, such as the very distinct peak at ~140°. This temperature is comparable to the surface melting transition reported for similar alkylsiloxane monolayers on silica.[37] From this information only we would be prone to address the change in colour to a change in the orientation at the particles surface. However, the analysis of the dimension of the assembly at different times before, after polymerization and at high temperature (Fig. 6) suggests that the network formed after polymerisation is rigid, since the assembly does not change its dimensions even at 150 °C. Therefore it would be unlikely that the sole change in the orientation at the particles would cause such a big effect on the network. For these reasons the birefringence was measured using a polarizing microscope equipped with a wedged compensation plate. The compensation of the birefringence of the sample was measured at 550 nm, and the thickness of the birefringent LC layer was determined using the optical interference method. The birefringence of the polymerised matrix is shown in Fig. 7b. It decreases with increasing temperature. The decrease is related to the decreasing order parameter with increasing temperature. For pure 5CB, the birefringence should abruptly decrease to zero at ~35 °C. Instead of the sharp discontinuity, the birefringence smoothly decreases up to 100 °C, where it gradually stabilizes at a small, but non-zero value. From the assessment of the birefringence we can therefore rule out the change in the alignment as a cause of the change in colour. A simultaneous change of the order at the particle and of the birefringence would result in no change in colour.[38,39]

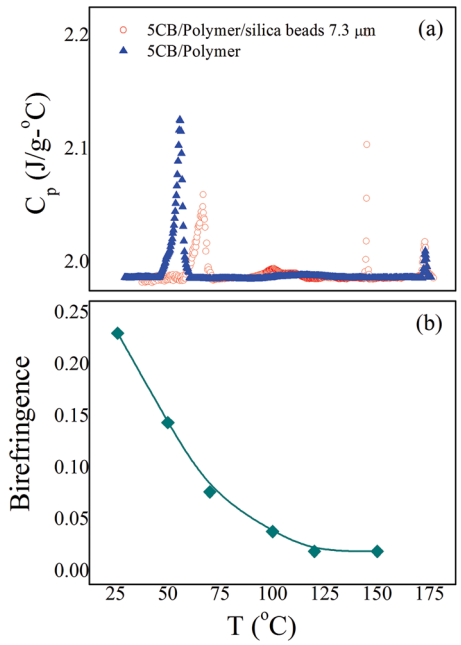

Fig. 7 (a) Temperature dependence of the heat capacity of the polymerized reactive-mesogen-5CB mixture, determined by AC calorimetry. The blue triangles correspond to 50 wt% of reactive mesogen in 5CB; the red circles correspond to 50 wt% in 5CB + 7.3 μm silica microspheres with DMOAP treated surfaces. (b) Temperature dependence of the birefringence of a polymerized reactive mesogen-5CB mixture, determined at 550 nm using a wedged compensation plate. The solid line is a guide to the eye only.

After polymerisation the transmission of visible light through the reactive mesogen-5CB matrix appears the same as before the polymerisation and the turbidity of the sample is small. This can be observed if laser light is directed onto the ordered colloidal crystal structure and the diffraction pattern is monitored. Fig. 8a shows the diffraction pattern of a He–Ne beam from the colloidal crystal shown in the right panel of this figure. One can clearly observe well defined diffraction peaks with little background scattering at small wave-vectors, indicating small scattering losses. These losses are quite dominant in highly birefringent nematic LCs (in this case due to the presence of 5CB) and are due to strong orientational fluctuations of the optical axis due to thermal excitation.

Free-standing assemblies embedded in the LC polymer network

While the optical properties of the polymerised reactive mesogen-5CB matrix with colloidal inclusions seem to be very good on a micro-scale, we were also interested in the nano-scale structure of this composite material. The nanoscale structure of the polymer network is important for many photonic applications, because it influences the degree of optical losses due to the scattering of light at surface imperfections. For example, total internal reflection at the interface of two materials with different refractive indices is used to guide and confine light in

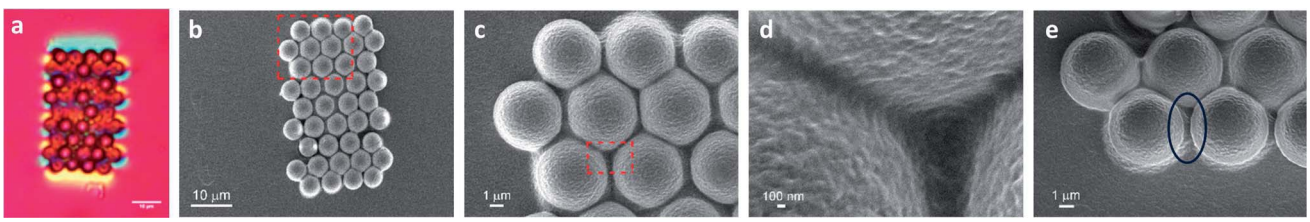

Fig. 8 (a) Reflection mode optical microscopy images of a colloidal crystal of 5 μm silica particles embedded in a polymerised nematic matrix after the unpolymerised LC was washed out, imaged between crossed polarizers with a retardation plate added; (b–d) SEM images of the same assembly at different magnifications; (e) SEM image of the assembly tilted by 12°. The blue ellipse indicates the region where topological defect is expected to be observed.

many photonic micro-devices. Here, the evanescent tail of the guided waves penetrates the material with a lower refractive index, and the optical smoothness of this interface at the scale of tens of nanometers is important. We therefore performed SEM analysis of the polymer network in the vicinity of colloidal surfaces.

The non-polymerized monomers and 5CB were washed out by soaking the cell in isopropanol for 2 days the cells was then opened carefully in order to have the polymer film all on one of the glasses. The polymer network was then observed with OPM and scanning electron microscopy (field emission SEM, JEOL 7600F; prior to the investigation the specimen was coated with a 3 nm thick layer of C using a Gatan's precision etching coating system). The optical polarised microscopy image in Fig. 9a (in reflection mode) shows an assembly of 5 μm colloids embedded in the polymer network. The distortion of the image is probably due to a partial detachment of the polymer network from the cell surface occurred when the cell was opened. SEM analysis (Fig. 8b–e) shows the high degree of organization of the colloid, even after the washing steps. SEM observation under a small angle (Fig. 8e) indicated that the polymer network clinged to the whole colloidal assembly and all the particles in the matrix. On an even smaller scale (Fig. 8d), one can see filament-like threaded polymer structure with a typical size of hundreds of nm. These present optical inhomogeneities on a nanoscale and could be problematic in terms of losses due to light scattering on frozen-in optical inhomogeneities. In spite of the fact that birefringence of the network is not observable with SEM, it is still possible to observe the general orientation of the network as is in some cases the presence of defects (Fig. 8e blue ellipse). Matrix polymerisation also provides the opportunity to use the colloidal crystals as free-standing objects otherwise only possible by lithographic techniques. We were able to peel the polymer film from the glass and observe an imbedded assembly under polarization microscope (Fig. 10). In this way the colloidal assemblies obtained with laser assisted assembly in LCs could be easily isolated and used for optical applications.

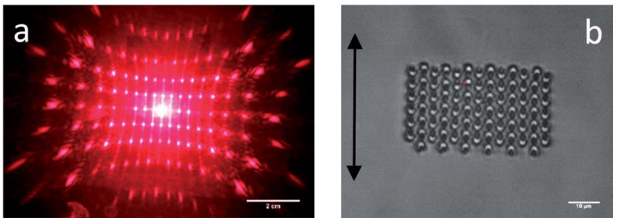

Fig. 9 (a) The diffraction pattern of a He–Ne laser beam from the colloidal assembly, shown in panel (b) constituted by 3.1 μm silica particles; the black arrow indicates the nematic director.

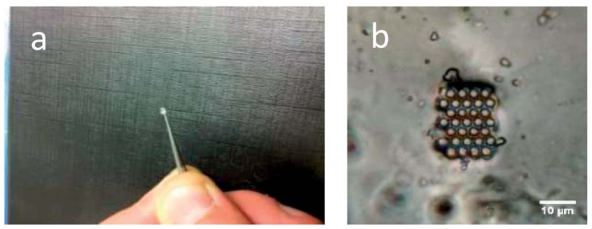

Fig. 10 (a) A portion of the polymer network film extracted from a cell. The portion contains a colloidal assembly which is shown in (b) imaged under a polarizing microscope with only the polarizer and without the analyser.

Conclusions

Here we present a proof-of-principle method on stabilization of colloidal crystals by means of photo-polymerisation of their liquid crystalline matrix. After assembly and matrix polymerisation, the colloids are dimensionally stable and the matrix retains its alignment also at high temperatures. We proved with calorimetric and birefringence studies that the polymer network is not affected by changes at the boundary, *i.e.* a change in the orientation at the surface of the particles. In addition, the assemblies can be extracted from the cell they are generated and isolated as free standing objects.

The method of stabilization of nematic colloidal structures by photo-polymerization could be applied to the assembling of liquid crystalline structures for photonic applications. It was recently demonstrated that various photonic microelements could be self-assembled from liquid crystals, such as Whispering Gallery Mode microlasers,[40] 3D microlasers,[41–43] tunable microresonators[44] and smectic-A optical fibers.[45] Based on this, it was recently proposed[46] that these photonic microelements could be assembled into soft matter photonic integrated microcircuits, where the flow of photons would replace the flow of electrons in traditional photonic microcircuits based on solid matter. Our method could therefore be used not only to stabilize the soft matter photonic microcircuits, but also to extract them from the assembling cells, therefore making them suitable for real application in photonics.

Acknowledgements

This research was supported by a Marie Curie Intra European Fellowship (Nemcode IEF-2012-331350) and a Marie Curie ITN (Hierarchy ITN 2007-215851) within the 7th European Community Framework Program. The authors are also grateful to Dr Miha Škarabot, Gregor Posnjak and Dr Andriy Nych for fruitful discussions and precious help with the experiments. We would also like to thank Merck Ltd. (Southampton, UK) for supplying the materials used for this study.

Notes and references

1 M. V. Landau, D. Tavor, O. Regev, M. L. Kaliya, M. Herskowitz, V. Valtchev and S. Mintova, *Chem. Mater.*, 1999, **11**, 2030–2037.
2 G. von Freymann, V. Kitaev, B. V. Lotsch and G. A. Ozin, *Chem. Soc. Rev.*, 2013, **42**, 2528–2554.
3 J. T. G. Overbeek, *Powder Technol.*, 1984, **37**, 195–208.
4 B. V. Derjaguin, *Prog. Surf. Sci.*, 1993, **43**, 109–114.
5 W. C. K. Poon, *J. Phys.: Condens. Matter*, 2002, **14**, R859–R880.

6 E. H. A. de Hoog, W. K. Kegel, A. van Blaaderen and H. N. W. Lekkerkerker, *Phys. Rev. E: Stat., Nonlinear, Soft Matter Phys.*, 2001, **64**, 021407.
7 S. Furumi, H. Fudouzi and T. Sawada, *Laser Photonics Rev.*, 2010, **4**, 205–220.
8 J. H. Zhang, Y. F. Li, X. M. Zhang and B. Yang, *Adv. Mater.*, 2010, **22**, 4249–4269.
9 H. L. Cong, B. Yu, J. G. Tang, Z. J. Li and X. S. Liu, *Chem. Soc. Rev.*, 2013, **42**, 7774–7800.
10 J. Liu, T. Y. Yang, D. W. Wang, G. Q. M. Lu, D. Y. Zhao and S. Z. Qiao, *Nat. Commun.*, 2013, **4**, 2798.
11 R. Rice, R. Roth and C. P. Royall, *Soft Matter*, 2012, **8**, 1163–1167.
12 S. Biffi, R. Cerbino, F. Bomboi, E. M. Paraboschi, R. Asselta, F. Sciortino and T. Bellini, *Proc. Natl. Acad. Sci. U. S. A.*, 2013, **110**, 15633–15637.
13 I. Muševič, *Philos. Trans. R. Soc., A*, 2013, **371**, 20120266.
14 H. Stark, *Phys. Rep.*, 2001, **351**, 387–474.
15 R. Pratibha and N. V. Madhusudana, *Mol. Cryst. Liq. Cryst.*, 1990, **178**, 167–178.
16 P. Poulin, H. Stark, T. C. Lubensky and D. A. Weitz, *Science*, 1997, **275**, 1770–1773.
17 I. Muševič, M. Škarabot, U. Tkalec, M. Ravnik and S. Žumer, *Science*, 2006, **313**, 954–958.
18 A. Nych, U. Ognysta, M. Škarabot, M. Ravnik, S. Žumer and I. Muševič, *Nat. Commun.*, 2013, **4**, 1489.
19 A. Ashkin, *Phys. Rev. Lett.*, 1970, **24**, 156–159.
20 D. C. Benito, D. M. Carberry, S. H. Simpson, G. M. Gibson, M. J. Padgett, J. G. Rarity, M. J. Miles and S. Hanna, *Opt. Express*, 2008, **16**, 13005–13015.
21 M. Yada, J. Yamamoto and H. Yokoyama, *Phys. Rev. Lett.*, 2004, **92**, 185501.
22 I. I. Smalyukh, A. N. Kuzmin, A. V. Kachynski, P. N. Prasad and O. D. Lavrentovich, *Appl. Phys. Lett.*, 2005, **86**.
23 I. Muševič, M. Škarabot, D. Babič, N. Osterman, I. Poberaj, V. Nazarenko and A. Nych, *Phys. Rev. Lett.*, 2004, **93**, 187801.
24 M. Škarabot, M. Ravnik, D. Babič, N. Osterman, I. Poberaj, S. Žumer, I. Muševič, A. Nych, U. Ognysta and V. Nazarenko, *Phys. Rev. E: Stat., Nonlinear, Soft Matter Phys.*, 2006, **73**, 021705.
25 M. Škarabot, Ž. Lokar and I. Muševič, *Phys. Rev. E: Stat., Nonlinear, Soft Matter Phys.*, 2013, **87**, 062501.
26 U. Tkalec, M. Ravnik, S. Čopar, S. Žumer and I. Muševič, *Science*, 2011, **333**, 62–65.
27 V. S. R. Jampani, M. Škarabot, M. Ravnik, S. Čopar, S. Žumer and I. Muševič, *Phys. Rev. E: Stat., Nonlinear, Soft Matter Phys.*, 2011, **84**, 031703.
28 P. Xie and R. B. Zhang, *J. Mater. Chem.*, 2005, **15**, 2529–2550.
29 Z. Q. Pei, Y. Yang, Q. M. Chen, E. M. Terentjev, Y. Wei and Y. Ji, *Nat. Mater.*, 2014, **13**, 36–41.
30 S. S. Choi, S. M. Morris, W. T. S. Huck and H. J. Coles, *Adv. Mater.*, 2010, **22**, 53–56.
31 Z. Hussain, A. Masutani, D. Danner, F. Pleis, N. Hollfelder, G. Nelles and P. Kilickiran, *J. Appl. Phys.*, 2011, **109**, 114513.
32 D. Dasgupta, I. K. Shishmanova, A. Ruiz-Carretero, K. B. Lu, M. Verhoeven, H. P. C. van Kuringen, G. Portale, P. Leclere, C. W. M. Bastiaansen, D. J. Broer and A. Schenning, *J. Am. Chem. Soc.*, 2013, **135**, 10922–10925.
33 Namely, a retardation plate, which is inserted between two crossed polarizers with its slow axis at 45°, gives the information on the local orientation of the liquid crystal molecules. This information is given by the color of that area. A thin layer of 5CB at room temperature appears yellow, when the 5CB molecules are oriented parallel to the slow axis of the retardation plate. Those regions of 5CB molecules, which are oriented perpendicular to the slow axis, appear blue. This sequence of colors repeats, if the optical path of light (*i.e.* the product of the sample thickness and the material birefringence) either increases or decreases. In LCs this change of colors usually happens, because the birefringence changes with temperature. Therfore, the change in color with increasing temperature does not indicate a change in the orientation of the nematic around the particles, but it is due to the change of the birefringence, which decreases with increasing temperature.
34 H. Yao, K. Ema and C. W. Garland, *Rev. Sci. Instrum.*, 1998, **69**, 172–178.
35 Z. Kutnjak, J. Petzelt and R. Blinc, *Nature*, 2006, **441**, 956–959.
36 M. Lavrič, V. Tzitzios, S. Kralj, G. Cordoyiannis, I. Lelidis, G. Nounesis, V. Georgakilas, H. Amenitsch, A. Zidanšek and Z. Kutnjak, *Appl. Phys. Lett.*, 2013, **103**, 143116.
37 M. CalistriYeh, E. J. Kramer, R. Sharma, W. Zhao, M. H. Rafailovich, J. Sokolov and J. D. Brock, *Langmuir*, 1996, **12**, 2747–2755.
38 U. Tkalec, M. Škarabot and I. Muševič, *Soft Matter*, 2008, **4**, 2402–2409.
39 I. I. Smalyukh, R. Pratibha, N. V. Madhusudana and O. D. Lavrentovich, *Eur. Phys. J. E: Soft Matter Biol. Phys.*, 2005, **16**, 179–191.
40 M. Humar and I. Musevic, *Opt. Express*, 2011, **19**, 19836–19844.
41 M. Humar and I. Muševič, *Opt. Express*, 2010, **18**, 26995–27003.
42 D. J. Gardiner, S. M. Morris, P. J. W. Hands, C. Mowatt, R. Rutledge, T. D. Wilkinson and H. J. Coles, *Opt. Express*, 2011, **19**, 2432–2439.
43 G. Cipparrone, A. Mazzulla, A. Pane, R. J. Hernandez and R. Bartolino, *Adv. Mater.*, 2011, **23**, 5773.
44 M. Humar, M. Ravnik, S. Pajk and I. Muševič, *Nat. Photonics*, 2009, **3**, 595–600.
45 K. Peddireddy, V. S. R. Jampani, S. Thutupalli, S. Herminghaus, C. Bahr and I. Musevic, *Opt. Express*, 2013, **21**, 30233–30242.
46 I. Muševič, *Liq. Cryst.*, 2013, **41**, 418–429.